

MULTIDIMENSIONAL COUPLED PHOTON-ELECTRON TRANSPORT SIMULATIONS USING NEUTRAL PARTICLE S_N CODES

Dan Ilas, Mark L. Williams, Douglas E. Peplow, and Bernadette L. Kirk

Oak Ridge National Laboratory

ilasd@ornl.gov; williamsml@ornl.gov; peplowde@ornl.gov; kirkbl@ornl.gov

ABSTRACT

During the past two years a study was underway at ORNL to assess the suitability of the popular S_N neutral particle codes ANISN, DORT and TORT for coupled photon-electron calculations specific to external beam therapy of medical physics applications. The CEPXS-BFP code was used to generate the cross sections. The computational tests were performed on phantoms typical of those used in medical physics for external beam therapy, with materials simulated by water at different densities and the comparisons were made against Monte Carlo simulations that served as benchmarks.

Although the results for one-dimensional calculations were encouraging, it appeared that the higher dimensional transport codes had fundamental difficulties in handling the electron transport. The results of two-dimensional simulations using the code DORT with an S_{16} fully symmetric quadrature set agree fairly with the reference Monte Carlo results but not well enough for clinical applications. While the photon fluxes are in better agreement (generally, within less than 5% from the reference), the discrepancy increases, sometimes very significantly, for the electron fluxes. The paper, however, focuses on the results obtained with the three-dimensional code TORT which had convergence difficulties for the electron groups. Numerical instabilities occurred in these groups. These instabilities were more pronounced with the degree of anisotropy of the problem.

KEYWORDS: discrete ordinates, electron transport, Monte Carlo

1. INTRODUCTION

The use of standard, neutral particle discrete ordinates codes to solve the transport of charged particles is highly desirable because of the wide availability and maturity of such codes.

The Boltzmann equation:

$$\hat{\Omega} \cdot \vec{\nabla} \psi(\vec{r}, E, \hat{\Omega}) + \sigma_t(\vec{r}, E) \psi(\vec{r}, E, \hat{\Omega}) = \int_0^\infty dE' \int_{4\pi} d\hat{\Omega}' \sigma_s(\vec{r}, E' \rightarrow E, \hat{\Omega} \cdot \hat{\Omega}') \psi(\vec{r}, E', \hat{\Omega}') + Q(\vec{r}, E) \quad (1)$$

can be used (with appropriate boundary conditions) to find the angular flux distribution throughout a domain of interest. However, in situations typical of electron transport, the cross sections are extremely anisotropic, with straight-ahead (close to $\theta = 0$ or $\mu_0 \equiv \hat{\Omega} \cdot \hat{\Omega}' = 1$) scattering cross sections being many orders of magnitude larger than the cross sections at wider

angles (for example, for $\mu \leq 0.8$). This creates major difficulties in using the Legendre expansion formalism, typical of S_N codes, because the number of Legendre terms needed to adequately represent the cross section would be huge (~ 1000).

A preferred approach to deal with the highly forward-peaked transport is to use the Boltzmann-Fokker-Planck (BFP) equation which is based on the decomposition of the scattering kernel into “regular” (wide angle scattering) and “singular” (forward-peaked scattering) components:

$$\sigma_s(\vec{r}, E \rightarrow E', \hat{\Omega} \rightarrow \hat{\Omega}') = \sigma_{s,reg}(\vec{r}, E \rightarrow E', \hat{\Omega} \rightarrow \hat{\Omega}') + \sigma_{s,sing}(\vec{r}, E \rightarrow E', \hat{\Omega} \rightarrow \hat{\Omega}') \quad (2)$$

The “regular” part is treated by the usual Legendre expansion, while the “singular” part incurs a different treatment. The BFP equation is thus obtained as

$$\begin{aligned} & \hat{\Omega} \cdot \vec{\nabla} \psi(\vec{r}, E, \hat{\Omega}) - \frac{\partial}{\partial E} [S(\vec{r}, E) \psi(\vec{r}, E, \hat{\Omega})] - \\ & \frac{1}{2} T(\vec{r}, E) \left\{ \frac{\partial}{\partial \mu} \left[(1 - \mu^2) \frac{\partial \psi(\vec{r}, E, \hat{\Omega})}{\partial \mu} \right] + \frac{1}{1 - \mu^2} \frac{\partial^2 \psi(\vec{r}, E, \hat{\Omega})}{\partial \varphi^2} \right\} + \sigma_t(\vec{r}, E) \psi(\vec{r}, E, \hat{\Omega}) = \\ & \int_0^\infty dE' \int_{4\pi} d\hat{\Omega}' \sigma_{s,reg}(\vec{r}, E' \rightarrow E, \hat{\Omega}' \cdot \hat{\Omega}) \psi(\vec{r}, E', \hat{\Omega}') + Q(\vec{r}, E) \end{aligned} \quad (3)$$

Where $S(\vec{r}, E)$ and $T(\vec{r}, E)$ are the restricted stopping power and the restricted momentum transfer, respectively. They are defined based on the “singular” part of the scattering kernel. The term containing the stopping power, second from left hand side of Eq. (3), is termed the continuous slowing down (CSD) term, and the term containing the momentum transfer, third from left hand side of Eq. (3), is the continuous scattering (CS) term.

The use of the BFP equation assumes modifications to the existing standard discrete ordinates codes to include the Fokker-Planck terms (energy and angular derivatives in Eq. 3) and will not be analyzed here.

Returning to the standard discrete ordinates codes, one way to reduce the magnitude of the scattering cross section is to separate the sharp peak at $\mu = 1$ by modeling it with a Dirac-delta function, $\delta(\mu - 1)$. If the Legendre expansion of the cross section is cut at the N^{th} order and the cross section moments are corrected by subtracting the $(N+1)^{\text{th}}$ moment, the P_{N+1} transport-corrected P_N expansion is obtained [1]. The moments so obtained are much smaller in magnitude, and the corrected scattering cross section is less forward-peaked. The method, used in conjunction with a Gauss quadrature in 1-D calculations, allows the use of a much smaller expansion order ($N \sim 10$) with very reasonable results.

A literature survey on the deterministic approach for electron or coupled photon-electron transport with existing neutral particle Boltzmann solvers evidenced that, while a rich literature exists for dealing with one-dimensional cases, little work was done for the multidimensional calculations. The seed paper for the one-dimensional calculations can be considered Morel’s 1981 paper [2]. Regarding the multidimensional cases, one exception is C.R. Drumm’s 1997

paper [3], which uses a Goudsmit-Saunders approach to prepare multigroup Legendre cross sections appropriate for the standard discrete ordinates codes. The Goudsmit-Saunders is limited to infinite-medium problems and neglects the hard-inelastic (wide angle) scattering.

The present study focuses on evaluating the TORT [4] discrete ordinates code for electron transport with cross-sections prepared by CPEXS-BFP [5], a modified version of the CPEXS code [6].

2. CROSS SECTIONS PREPARATION

The CEPXS-BFP code [5] was contributed to the Radiation Safety Information Center (RSICC) at ORNL by the Russian Academy of Sciences Keldysh Institute of Applied Mathematics. This code has the capability of producing data needed for explicit Fokker-Planck treatment, as well as indirect treatments such as in the original CEPXS (the CEPXS-GS method of ref. [3] is not available).

The following three options are available in CEPXS-BFP:

- (1) “S_N-CSD” Produces restricted stopping powers at the multigroup energy boundaries, for transport codes that explicitly treat the CSD term using diamond differencing, but represents the CS angular operator indirectly by Legendre expansion.
- (2) “S_N-BFP” Produces restricted stopping powers and restricted momentum transfer coefficients for transport codes that explicitly treat both CSD and CS differential operators using finite difference.
- (3) “S_N-Indirect” Produces data for transport codes that indirectly treat both the CSD and CS operators by including modified cross sections in the standard multigroup library. This approach is nearly identical to the CEPXS methodology, but the results are in a different format.

The CEPXS-BFP code was used to produce electron interaction data for the ORNL transport codes in this project.

In the “S_N-indirect” option the total and scattering cross sections for use in the standard discrete ordinates codes are redefined for a P_L expansion as:

$$\tilde{\sigma}_t^g = \sigma_{t,BFP}^g + \frac{T^g}{2} L(L+1) + \frac{2S_{g+1/2}}{\Delta E_g} \quad (4)$$

$$\tilde{\sigma}_{s,l}^{g' \rightarrow g} = \sigma_{s,l,BFP}^{g' \rightarrow g} + \frac{T^g}{2} [L(L+1) - l(l+1)] \delta_{g'g} + \frac{(-1)^{g'-g+1} 2(S_{g-1/2} + S_{g+1/2})}{\Delta E_g}, \quad \text{for } g' \leq g \quad (5)$$

where the BFP-labeled terms are the terms that would be used in a BFP treatment (in case of the scattering kernel it represents the Legendre moment for the “regular” part of the scattering cross-section). The sum of the first two terms in Eqs. (4) and (5) represent the CSD cross sections that are generated with the “S_N-CSD” option, which explicitly uses the stopping power.

The preferred approach in this study, however, was to use the “S_N-CSD” cross sections and embed the stopping power term by post processing in the ARVES2.5 code [7]. This code uses a

weighted 2-step scheme in energy to incorporate the stopping power. The resulting cross sections that are to be used in the standard codes are defined as:

$$\tilde{\sigma}_t^g = \sigma_{t,CSD}^g + \frac{S_{g+1/2}}{\Delta E_g} \left(1 + \frac{P_g}{2} \right) \quad (6)$$

$$\tilde{\sigma}_{s,l}^{g' \rightarrow g} = \sigma_{s,l,CSD}^{g' \rightarrow g} + \sigma_S^{g' \rightarrow g}, \quad \text{for } g' = g-1, g-2 \quad \text{where}$$

$$\sigma_S^{g-1 \rightarrow g} = \frac{\left(S_{g-1/2} \left(1 + \frac{P_{g-1}}{2} \right) + S_{g+1/2} \frac{P_g}{2} \right)}{\Delta E_{g-1}}, \quad \sigma_S^{g-2 \rightarrow g} = -\frac{P_{g-1}}{2\Delta E_{g-2}} S_{g-1/2} \quad (7)$$

The cross sections were generated on 40 electron groups (and 40 photon groups).

3. RESULTS

3.1. Problem description

Calculations were performed on a fully 3-D, realistic human phantom provided by the University of North Carolina. The full depth of the phantom (62 voxels, 0.4 cm in size) was used along the y direction, but only a region 20x20 voxels wide was used for the cross sectional x-z plane (Fig. 1).

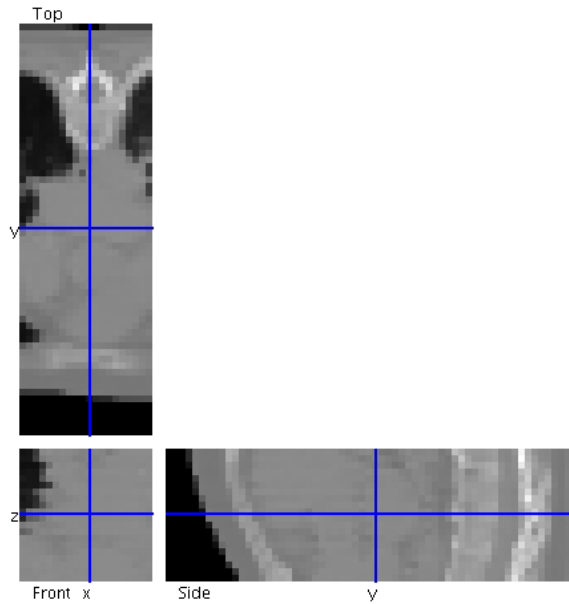


Figure 1. Cross sectional views through the computational phantom

To capture the scattering of the electrons which is assumed to be very forward peaked, we used a quadrature with such forward peaking features. This forward biased quadrature had a total of 560 directions pointing forward and 70 directions pointing backwards.

The photon source is modeled as a surface source (at $y=9.576\text{cm}$ on the original phantom, i.e. minimum y value) with a spectrum typical of a radiotherapy source and is assumed to emit

photons within a 30° cone of directions (15° with respect to the y axis) in which a large number of quadrature set directions lay. The source's spatial extension is constrained to a 10×10 voxel square, central on the plane perpendicular to the depth (xz plane for the original phantom). This set up allows for testing the behavior of TORT on a more realistic case, with a non-isotropic source and a sharp spatial gradient in the penumbra region.

3.2. Three dimensional results

The Monte-Carlo code EGSnrc [8] was used as reference and we compared the ratio TORT/EGS for the total photon flux and the total electron flux throughout the phantom. Figure 2 shows these ratios for a cut plane $z=15\text{cm}$. The photon source is at the bottom and impinges upwards. Ideally, the TORT/EGS flux ratio should be constant (i.e. solid color). With appropriate normalization between TORT and EGSnrc this ratio should be 1 throughout. However, because of the numerical problems in TORT (and to a lesser extent because of the statistical errors in EGSnrc), the ratio of the fluxes computed by TORT and EGSnrc is not constant. For photons, the variation is about 5% in most of the phantom with an underestimation by TORT in regions close to the source's axis and an overestimation towards the periphery of the source beam region. For the electron fluxes ratio the variation is still around 5% in most of the phantom (with appropriate rescaling – the variation within one unique color on Figure 2 right is about $\pm 4\%$) with an underestimation in the central region. The electron flux ratio decreases in regions which are further away from the source. The most fundamental problem, however, was that while the ratio for photons was reasonably close to 1, the ratio for electron fluxes was orders of magnitude different.

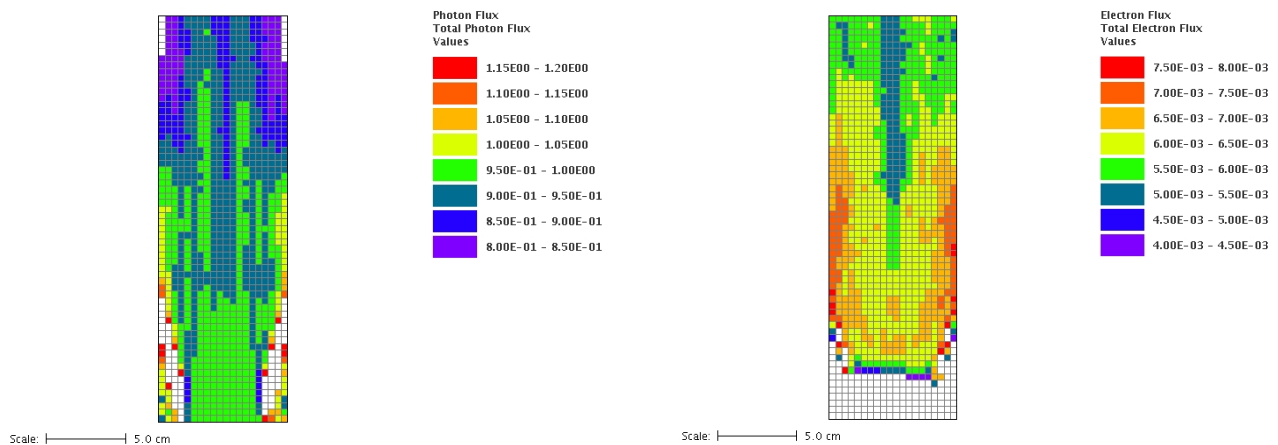


Figure 2. The ratio TORT/EGS for the total photon (left) and electron fluxes at $z=15\text{cm}$

The above scoping results were obtained using 2 inner iterations per energy group. The computational time was about half of that used for EGSnrc to achieve a reasonable relative error (below 5%).

Difficulties in the electron group's convergence were found when we attempted to increase the number of iterations for each energy group. The solution may diverge after a target number of iterations. Figure 3 shows that ratio TORT/EGS for the photon fluxes along a central depth line. It can be noticed that the curves for 2 and 4 iterations per energy group practically overlap. Over the whole phantom, raising the number of iterations to 4 for the photon groups leads to changes

smaller than 1% in the flux distribution. When the quadrature set was changed to the S_{16} fully symmetric, difficulties began to show up even for the photons, because there were too few directions within the 30° cone (only 4 non-zero weighted directions, compared to 440 directions for the biased set) to adequately capture the highly forward-peaked fluxes. The disagreement for the S_{16} fully symmetric quadrature starts only after a few centimeters from the source.

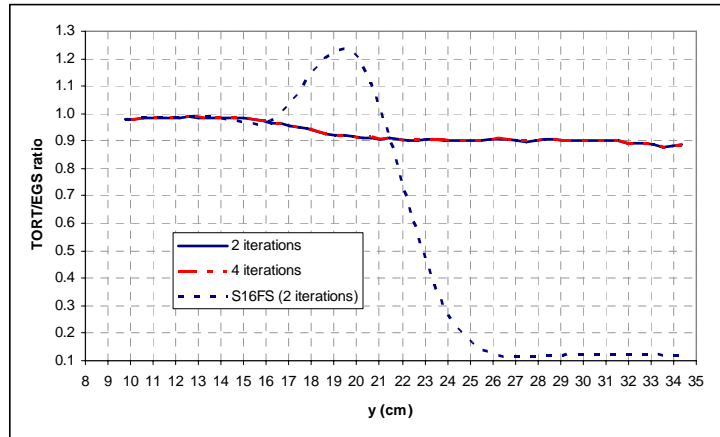


Figure 3. The TORT/EGS ratio for photon fluxes along a central depth line for three calculations

Fundamental convergence difficulties are observed for the electron groups when the number of iterations is increased. Figure 4 exposes a resonance-like increase in the electron flux at some point along the central depth axis. The S_{16} fully symmetric set also has difficulties in handling the electrons.

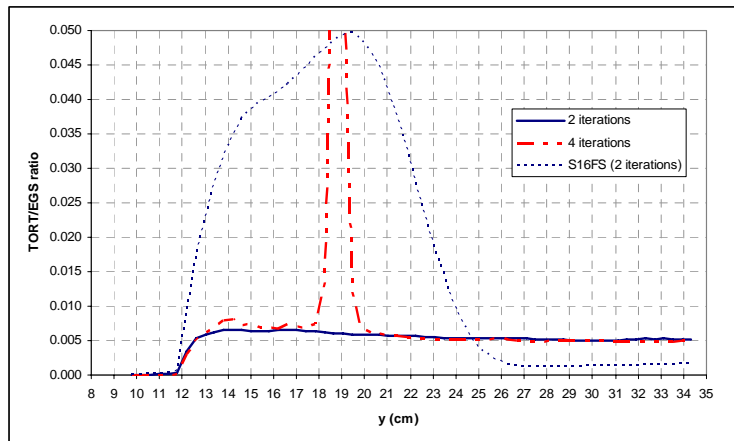


Figure 4. The TORT/EGS ratio for electron fluxes along a central depth line for three calculations

Figure 5 shows how the numerical instability has propagated throughout the phantom when the number of inner iterations is increased. The red color shows a divergence in electron flux errors, probably due to the difficulties in handling large spatial gradients.

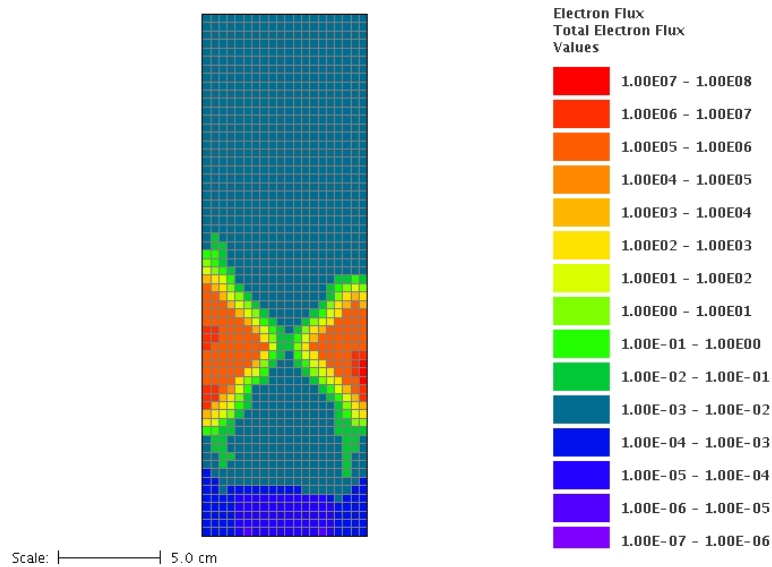


Figure 5. The ratio TORT/EGS for the total electron flux at $z=15\text{cm}$

In conclusion, the tests show that the ORNL's three-dimensional discrete ordinates transport code TORT has fundamental convergence difficulties in transporting the electrons with the electron cross sections derived according to the CEPXS methodology. Because of this, it is not possible to make meaningful comparisons for the 3D electron transport case.

4. CONCLUSIONS

Although reasonable good agreement was obtained for one-dimensional calculations for both photon and electron transport, it appears that the higher dimensional standard discrete ordinates transport codes have fundamental difficulties in handling the electron transport.

The three dimensional code TORT had fundamental convergence difficulties for electrons. On configuration with an isotropic source, the two dimensional code DORT [9] gave results (not shown in this paper) close to the reference Monte Carlo but not enough for clinical applications. An S16 fully symmetric quadrature set was used for the DORT calculations.

It appears that the difficulties stem from the cross section preparation. A deeper insight into this issue is necessary.

The computational time for the discrete ordinates calculations compared well against Monte Carlo for the problems considered. It should be noticed that the codes used are general purpose codes, not specialized for voxelized geometries. Specializing the codes for this type of geometry could lead to significant gains in computational speeds.

As a final conclusion, the explicit (direct) treatment of the Fokker-Planck terms is recommended when dealing with the electron transport.

ACKNOWLEDGMENTS

The study was partially funded by the National Cancer Institute (NCI) of the National Institutes of Health (NIH) under Grant Number R21 CA114614.

The authors want to acknowledge the help of Dr. Charles O. Slater in setting up the TORT input files.

REFERENCES

1. J.E. Morel, "On the Validity of the Extended Transport Cross-Section Correction for Low-Energy Electron Transport", *Nuclear Science and Engineering*, **71**, pp.64-71 (1979).
2. J.E. Morel, "Fokker-Planck Calculations Using Standard Discrete Ordinates Transport Codes", *Nuclear Science and Engineering*, **79**, pp.340-356 (1981).
3. C.R. Drumm, "Multidimensional Electron-Photon Transport with Standard Discrete Ordinates Codes", *Nuclear Science and Engineering*, **127**, pp.1-21 (1997).
4. W. A. Rhoades and R. L. Childs, *The TORT Three-Dimensional Discrete Ordinates Neutron/Photon Transport Code*, ORNL-6268, Oak Ridge National Laboratory (1987).
5. A. M. Voloschenko, "CEPXS-BFP: Version of Multigroup Coupled Electron-Photon Cross-Section Generation Code CEPXS Adapted for Solving the Charged Particle Transport in the Boltzmann-Fokker-Plank Formulation with the Use of Discrete Ordinate Method User's Guide," Report No. 7-36-2004, Keldysh Inst. of Appl. Math., Russian Ac. of Science, Moscow (2004).
6. L. J. Lorence, J. E. Morel, and G. D. Valdez, "Physics Guide to CEPXS/ONELD: A Multigroup Coupled Electron-Photon Cross Section Generating Code," SAND89-1685, Sandia National Laboratories (1989).
7. A. M. Voloschenko, S. V. Gukov, and A. V. Shwetsov, "ARVES-2.5: Preprocessor for the Working Macroscopic Cross-Section FMAC-M Format for Transport Calculations User's Guide," Rept. No. 7-24-2004, Keldysh Inst. of Appl. Math., Russian Ac. of Science, Moscow (2004).
8. I. Kawrakow, "Accurate Condensed History Monte Carlo Simulation of Electron Transport. I. EGSnrc, the new EGS4 version," *Medical Physics*, **27**, 485 (2000)
9. W. A. Rhoades and R. L. Childs, "The DORT Two-Dimensional Discrete Ordinates Transport Code," *Nuclear Science and Engineering*, **99**, 88-89 (May 1988).